ORIGINAL PAPER

Two birds with one stone: integrating exfoliation and immunoaffinity properties in multi-walled carbon nanotubes by non-covalent functionalization with human immunoglobulin G

Michael López Mujica[1] · **Alejandro Tamborelli**[1,2] · **Virginia M. Vaschetti**[2] · **L. Carolina Espinoza**[3,4] · **Soledad Bollo**[3,4] · **Pablo R. Dalmasso**[2] · **Gustavo A. Rivas**[1]

Abstract

An innovative strategy is proposed to simultaneously exfoliate multi-walled carbon nanotubes (MWCNTs) and generate MWCNTs with immunoaffinity properties. This strategy was based on the non-covalent functionalization of MWCNTs with human immunoglobulin G (IgG) by sonicating 2.5 mg mL^{-1} MWCNTs in 2.0 mg mL^{-1} IgG for 15 min with sonicator bath. Impedimetric experiments performed at glassy carbon electrodes (GCE) modified with the resulting MWCNT-IgG nanohybrid in the presence of anti-human immunoglobulin G antibody (Anti-IgG) demonstrated that the immunoglobulin retains their biorecognition properties even after the treatment during the MWCNT functionalization. We proposed, as proof-of-concept, two model electrochemical sensors, a voltammetric one for uric acid quantification by taking advantages of the exfoliated MWCNTs electroactivity (linear range, 5.0×10^{-7} M - 5.0×10^{-6} M; detection limit, 165 nM) and an impedimetric immunosensor for the detection of Anti-IgG through the use of the bioaffinity properties of the IgG present in the nanohybrid (linear range, 5-50 μg mL^{-1}; detection limit, 2 μg mL^{-1}).

Michael López Mujica and Alejandro Tamborelli contributed equally to this work.

✉ Pablo R. Dalmasso
pdalmasso@frc.utn.edu.ar; p-dalmasso@hotmail.com

✉ Gustavo A. Rivas
gustavo.rivas@unc.edu.ar

1 INFIQC (CONICET-UNC), Departamento de Fisicoquímica, Facultad de Ciencias Químicas, Universidad Nacional de Córdoba, Ciudad Universitaria, 5000 Córdoba, Argentina

2 CIQA, CONICET, Departamento de Ingeniería Química, Facultad Regional Córdoba, Maestro López Esq, Universidad Tecnológica Nacional, Cruz Roja Argentina, 5016 Córdoba, Argentina

3 Centro de Investigación de Procesos Redox, CIPRex, Facultad de Ciencias Químicas Y Farmacéuticas, Universidad de Chile, Santiago, Chile. Sergio Livingstone 1007, Independencia, Santiago, Chile

4 Departamento de Química Farmacológica Y Toxicológica, Facultad de Ciencias Químicas Y Farmacéuticas, Universidad de Chile, Sergio Livingstone 1007, Independencia, Santiago, Chile

Introduction

The development of (bio)sensing platforms with improved analytical performance is one of the current challenges in the electrochemical sensors field. Nanomaterials have emerged as unique constituents of advanced electrochemical sensors, participating in the construction of the recognition layer and/or in the transduction event [1–4]. In this context, carbon nanotubes (CNTs) have proven to be an excellent material for the development of innovative and versatile electrochemical (bio)sensors due to their unique electronic, physical, and chemical properties, their high chemical stability and their capability to be functionalized following different schemes [5–8]. However, to reduce the strong tendency of the CNTs to form bundles due to van der Waals and π-π interactions and to improve their compatibility with the solvent without disturbing their π-conjugated structure, a functionalization step is highly required [9–11]. In this regard, the non-covalent functionalization of CNTs involving biomolecules has been successfully used to obtain exfoliated CNTs with special biorecognition properties [12]. We reported the use

of glucose oxidase [13], calf-thymus double stranded DNA [14–16], avidin [17–20], and concanavalin A [21] to functionalize multi-walled carbon nanotubes (MWCNTs) and obtain nanohybrids able to recognize glucose [13], promethazine [15], biotinylated enzymes [17, 18] or nucleic acids [19, 20], and glycoproteins [21], respectively.

In this work, we are proposing for the first time the non-covalent functionalization of MWCNTs with human immunoglobulin G (IgG) with two goals, to disaggregate the MWCNTs and to provide them of immunosensing/bioaffinity properties. To the best of our knowledge, there are no reports about the non-covalent functionalization of MWCNTs with IgG to obtain nanohybrids able to be used for the development of electrochemical (bio)sensors. There are two previous reports focused on biological implications of the interaction between CNTs and plasma proteins. Zhang et al. [22] studied the mechanisms underlying the interactions of bovine serum albumin (BSA) and IgG on MWCNT surfaces (using aqueous suspensions sonicated for 30 min in a bath sonicator) and the influence that this interaction could have on the cellular uptake, cytotoxicity and cellular responses, to enhance MWCNT biocompatibility and develop approaches for managing MWCNT hazards. They reported a strong π–π stacking interaction between pristine MWCNTs and aromatic protein residues which led to conformational changes in the protein. Lu et al. [23] investigated the binding of IgG, human serum albumin, and fibrinogen to single-walled carbon nanotubes (SWCNTs), using suspensions incubated for 2 h at 37 °C, and studied the effects of these different protein coronas on the cytotoxicity to endothelial cells and immune response to neutrophils in the bloodstream. They found that only the treatment of SWCNTs with IgG produced an enhancement of CNT-induced myeloperoxidase release in neutrophils, while myeloperoxidase-dependent degradation of CNTs induced less cytotoxicity than initial nanomaterials.

In the following sections, we report the characterization of the MWCNT-IgG nanohybrid using different techniques, the optimization of the preparation conditions, and the proof-of-concept of the analytical applications of glassy carbon electrodes (GCE) modified with this nanohybrid in connection with a voltammetric sensor for uric acid (UA) and a model impedimetric immunosensor for the detection of anti-human immunoglobulin G antibody (Anti-IgG).

Experimental

Reagents

MWCNTs (O.D., 6–13 nm; L, 2.5–20 μm; purity > 98%), uric acid (UA), bovine serum albumin (BSA), immunoglobulin G (IgG) from human serum (catalog number I4506), anti-human immunoglobulin G antibody (Anti-Ig G) (Fc

specific) produced in goat (catalog number I2136), hydroquinone (HQ), benzoquinone (BQ), thrombin, cytochrome c, and ferrocenemethanol (FcOH) were supplied by Sigma-Aldrich. Ascorbic acid (AA) and hydrogen peroxide (H_2O_2) (30% v/v aqueous solution) were acquired from Anedra and Cicarelli, respectively. All reagents used were analytical grade.

Ultrapure water ($\rho = 18.2$ MΩ cm) from a Millipore-MilliQ system was used for preparing all aqueous solutions.

Apparatus

A standard three-electrode system was used for all electrochemical measurements: glassy carbon electrode modified with nanohybrid as working electrode, a platinum wire as counter electrode, and a Ag/AgCl (3.0 M NaCl) (BAS) as reference electrode. All potentials are referred to this electrode. Amperometric and voltammetric experiments were performed with a TEQ_04 potentiostat. Electrochemical impedance spectroscopy (EIS) was carried out with a PGSTAT30 potentiostat (Methrom). Impedimetric measurements were performed using 1.0×10^{-3} M HQ/BQ as redox marker, which was prepared in 0.050 M phosphate buffer solution pH 7.40. The following parameters were used during EIS experiments: amplitude, 0.010 V; frequency range, from 1.0×10^{-2} to 1.0×10^{6} Hz; and working potential, 0.200 V. The Nyquist plots obtained from EIS experiments were analyzed and fitted using Zview program.

Sonication was performed with a TB04TA Testlab Ultrasonic Cleaner of 40 kHz frequency and 160 W ultrasonic power.

Fourier transform infrared (FTIR) spectra were obtained with a Nicolet FTIR spectrometer (2.0 cm^{-1} resolution, 32 scans) by drop-coating and drying the samples on a ZnSe disk (Pike Technologies, 25×4 mm).

Scanning electron microscopy (SEM) pictures were obtained with a field emission gun scanning electron microscope (FE-SEM, Zeiss, ΣIGMA model). The samples were placed over GCE disks and air dried at room temperature.

Scanning electrochemical microscopy (SECM) experiments were carried out using a CHI900 microscope (CH Instruments Inc., USA) with a platinum ultramicroelectrode (tip) of 25 μm of diameter. Before performing the approach curves, the tip surface state was checked by cyclic voltammetry in a 5.0×10^{-4} M FcOH solution (prepared in 0.050 M phosphate buffer solution pH 7.40). SECM experiments were performed using the feedback mode and FcOH as redox mediator. The tip potential was held at 0.500 V to permit the oxidation of FcOH, while the potential of the modified GCE (called substrate) was kept at 0.000 V to allow the feedback between the electrodes. Part of the MWCNT-IgG hybrid (around the half of the surface) was removed from the substrate, and the approach curve was conducted on the exposed

GCE surface at a tip scan rate of 0.5 μm s^{-1}. The tip stopped automatically when the steady-state tip current (i_T) reached 1.25 times the current obtained when the redox mediator is oxidized at the tip far away from the modified GCE ($i_{T,\infty}$). According to the theoretical curve that describes the dependence of i_T with the distance between the tip and the substrate (d), 1.25 times of $i_{T,\infty}$ corresponds to a $d \approx 25$ μm for a tip of 12,5 μm radius [24]. Subsequently, SECM images of 200×200 μm were recorded at a tip scan rate of 1 μms^{-1}. The results are presented in the dimensionless form of normalized current (I_T), by normalizing the experimental feedback current (i_T) with the steady-state current obtained when the tip was far from the substrate ($i_{T,\infty}$), i.e., $I_T = i_T/i_{T,\infty}$.

Preparation of MWCNT-IgG hybrid and GCE/MWCNT-IgG platform

To functionalize MWCNTs with IgG, 2.5 mg of MWCNTs was mixed with 1.0 mL of an aqueous solution of 2.0 mg mL^{-1} IgG. This mixture was sonicated for 15 min in ultrasonic bath obtaining, thus, MWCNT-IgG nanohybrid (Fig. 1A).

Before modification with the hybrid, GCEs were polished with 1.0, 0.3, and 0.05 μm alumina slurries for 2.0 min each, rinsed with deionized water, and dried with nitrogen stream. Then, an aliquot of 10 μL of MWCNTs-IgG was placed over the top of the polished GCEs, and it was left to dry at room temperature. Figure 1B shows a scheme of the electrode modification.

Analytical applications of GCE/MWCNT-IgG

For the quantification of Anti-IgG, the GCE/MWCNT-IgG electrode was washed with 0.050 M phosphate buffer solution pH 7.40 and then immersed in 100 μL of 2.0% BSA solution for 20 min to avoid non-specific adsorptions. Afterwards, it was rinsed with 0.050 M phosphate buffer solution pH 7.40. The immunodetection was performed by interaction of GCE/MWCNT-IgG with 20 μL of Anti-IgG solution deposited at the top of the electrode for 30 min. Before performing the EIS measurements, GCE/MWCNT-IgG⋯Anti-IgG was washed with 0.050 M phosphate buffer solution pH 7.40 and then immersed in the redox marker solution.

The electrochemical determination of UA was performed by adsorptive stripping with linear sweep voltammetry (LSV) transduction. UA was preconcentrated at open circuit potential (OCP) for 10 min, and after washing with 0.050 M phosphate buffer solution pH 7.40, the electrode was transferred to a fresh buffer solution to perform the LSV-stripping analysis by scanning the potential between −0.300 and 0.500 V at 0.100 V s^{-1}.

Results and discussion

Characterization of MWCNT-IgG nanohybrid

Cyclic voltammetry

Figure 2A displays ten successive cyclic voltammograms performed at 0.100 V s^{-1} between −0.300 V and 1.000 V at GCE/MWCNT-IgG in 0.050 M phosphate buffer solution pH 7.40. The first cycle shows one current peak at 0.820 V due to the irreversible oxidation of the tyrosine residues of the protein [25, 26], clearly indicating that the IgG is present at the electrode surface and, therefore, that it interacts with the MWCNTs. The negative scan shows a current peak at 0.104 V while the second cycle presents a new oxidation current peak at 0.189 V. As the number of cycles increases, the quasi-reversible peaks system at 0.104 V/0.189 V is better defined, while the current at 0.820 V continues decreasing. In order to obtain more information about this electrochemical behavior, GCE/MWCNT-IgG was cycled for ten times between -0.300 V and 0.500 V, as depicted in Fig. 2B. No peaks are observed under these conditions, confirming that the peak at 0.104 V is due to the reduction of the quinonoid compound obtained as primary oxidation product of tyrosine, while the one at 0.189 V corresponds to the re-oxidation of the compound reduced at 0.104 V [25, 26].
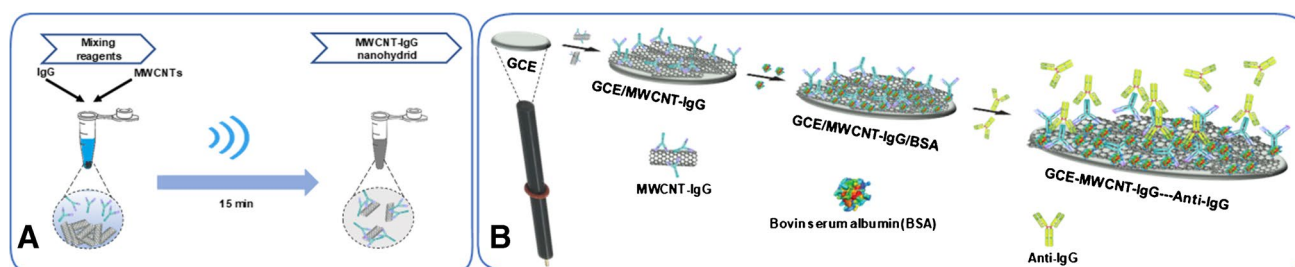

Fig. 1 Schematic representation of **A)** the preparation of MWCNT-IgG hybrid and **B)** the modification of GCE surface with the nanohybrid

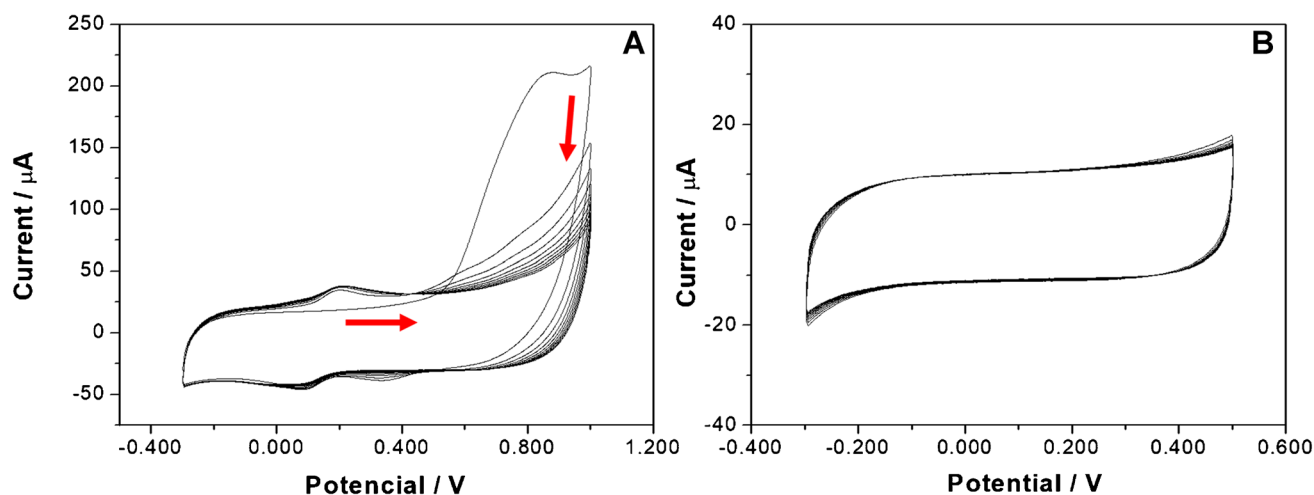**Fig. 2** Ten successive cyclic voltammograms obtained at GCE/MWCNT-IgG in a 0.050 M phosphate buffer solution pH 7.40 between −0.300 V and 1.000 V (**A**) and −0.300 V and 0.500 V (**B**). Scan rate: 0.100 V s^{-1}.[1]
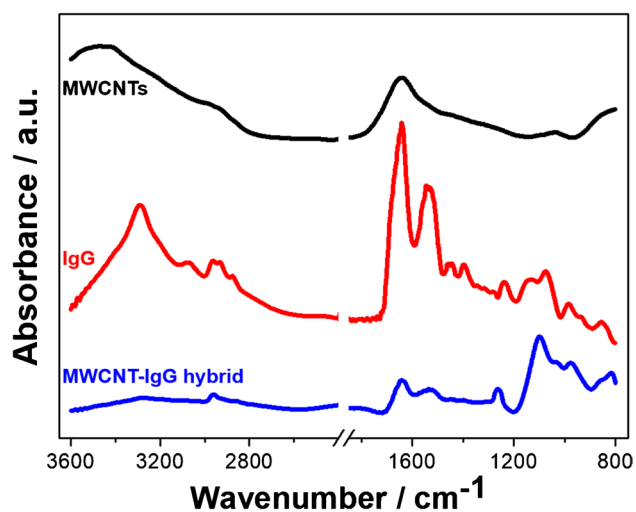

Fig. 3 FTIR spectrum for MWCNTs (black line), IgG (red line), and MWCNT-IgG nanohybrid (blue line). The spectra were recorded in triplicate

FTIR

Figure 3 displays FTIR spectra for MWCNTs (black line), IgG (red line), and MWCNT-IgG hybrid (blue line). The MWCNTs spectrum shows its characteristic weak band at 1640 cm^{-1} attributed to C=C stretching of phenyl ring vibrations, confirming the graphite structure of unmodified carbon nanotubes (the spectrum was magnified in order to show more clearly this contribution). IgG spectrum shows the typical absorption bands of amide I at ∼ 1640 cm^{-1} and amide II at ∼ 1530 cm^{-1}, a set of weaker bands between 1450 and 1230 cm^{-1} that represents amide III vibration modes, and a broad absorption band of amide A centered

at 3290 cm^{-1}. The absorption associated with amide I and amide II corresponds mainly to C=O stretching and N–H in-plane bending vibrations, respectively, while the amide A band is associated to N–H stretching vibrations [27]. The IR spectrum for MWCNT-IgG hybrid displays the characteristic bands of IgG, confirming the successful functionalization of the carbon nanomaterial with the protein. Minimum shifting of these bands allows to point out that IgG retains its near-native structure.

SEM

Figure S1 displays SEM images for glassy carbon disks modified with 2.5 mg mL^{-1} MWCNTs dispersed in water (A) and in 2.0 mg mL^{-1} IgG (B). As can be seen in Figure S1A at 750X magnification, the glassy carbon surface modified with carbon nanotubes dispersed in water shows bundles of MWCNTs distributed like in an islands pattern. At variance with this image, the glassy carbon disk modified with MWCNT-IgG nanohybrid displays a surface completely covered by the nanostructures, with areas containing a higher density of MWCNTs (Fig. S1B). Furthermore, the micrograph shown in the inset, which was obtained at 15KX, confirms the considerably low aggregation of the nanostructures on the glassy carbon modified with the MWCNT-IgG hybrid.

SECM

The electroactivity and topography of GCE modified with MWCNT-IgG nanohybrid were evaluated by SECM using FcOH as redox probe. Figure 4 depicts SECM images obtained at GCE modified with 2.5 mg mL^{-1} MWCNTs dispersed in: water (A), 0.5 mg mL^{-1} IgG (B),
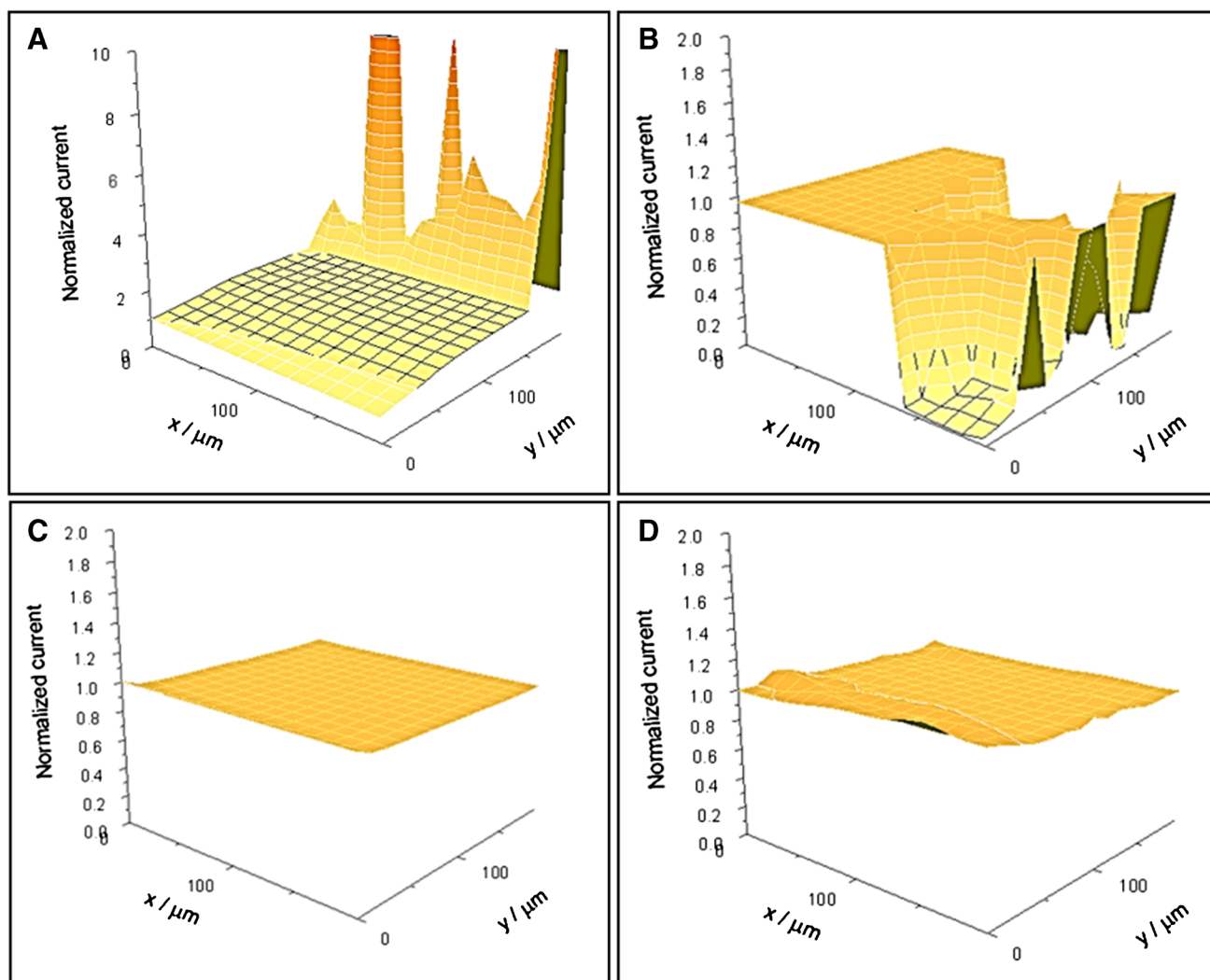
Fig. 4 SECM surface-plot images of GCE modified with 2.5 mg mL^{-1} MWCNTs dispersed in **A)** water, **B)** 0.5 mg mL^{-1} IgG, **C)** 1.5 mg mL^{-1} IgG, and **D)** 2.0 mg mL^{-1} IgG. Supporting electro-lyte, 0.050 M phosphate buffer pH 7.40; tip, platinum of 25 μm diameter; image parameters, 200×200 μm at 1 μm s^{-1} tip scan. Redox mediator: 5.0×10^{-4} M FcOH solution

1.5 mg mL^{-1} IgG (C), and 2.0 mg mL^{-1} IgG (D). GCE modified with MWCNTs dispersed in water shows areas with different electroactivity (Fig. 4A). Most of the surface presents i_T close to bare glassy carbon ($1.25 \times i_{T,\infty}$) and corresponds to the uncovered surface. Small regions have I_T several times higher than that observed for GCE ($i_T > i_{T,GCE}$), which are associated to the islands of MWCNT bundles poorly dispersed by water, in agreement with SEM images. On the contrary, GCE/MWCNT-IgG surfaces (Figs. 4 B, C, and D) present different patterns according to the IgG concentration. At glassy carbon modified with MWCNTs dispersed in 0.5 mg mL^{-1} IgG is possible to observe areas with i_T around 1.0 and others with values considerably lower. Taking into account that the aggregates of MWCNTs are visualized in the dispersion, the areas with higher I_T could correspond to

MWCNTs partially exfoliated by IgG, while those with very low I_T could be due to the blocking effect of IgG which is not sufficient to interact efficiently with such a large amount of MWCNTs. As the IgG concentration increases to 1.5 mg mL^{-1}, there is a significant change in the SECM pattern (Fig. 4C). There is a homogeneous topography due to the considerably better exfoliation of carbon nanotubes by IgG, indicating that the blocking effect of IgG is partially neutralized by the electroactivity of the exfoliated carbon nanostructures. The modification of GCE with a nanohybrid prepared using 2.0 mg mL^{-1} IgG (Fig. 4D) gives a surface similar to the one obtained using 1.5 mg mL^{-1} IgG, with i_T around 1.0 and some small areas with slightly higher i_T, which can be correlated with the existence of regions with high density of exfoliated MWCNTs, in agreement with SEM images.

Optimization of the nanohybrid preparation

We evaluate the influence of different experimental conditions on the efficiency of IgG to exfoliate MWCNTs by amperometry using hydrogen peroxide as redox indicator.

Effect of the concentration of IgG and MWCNTs

Figure 5A displays the effect of the IgG concentration used to prepare the nanohybrid (between 1.0 and 2.5 mg mL^{-1}) for different amounts of MWCNTs, 1.5 (a), 2.0 (b), 2.5 (c), and 3.0 (d) mg mL^{-1}, on the sensitivity for hydrogen peroxide oxidation at 0.700 V. The analysis of the figure allows to obtain interesting information: (i) the sensitivity for hydrogen peroxide increases with the amount of MWCNTs, demonstrating the efficient exfoliating capability of IgG even for 3.0 mg mL^{-1} MWCNTs; (ii) for a given amount of MWCNTs, the sensitivity increases with the concentration of IgG up to 2.0 mg mL^{-1}, even when the protein presents blocking characteristics, indicating that the most important effect is the electroactivity of the exfoliated MWCNTs that counteracts the blocking effect of the protein; (iii) for IgG concentrations higher than 2.0 mg mL^{-1}, the sensitivity decreases for all the concentrations of MWCNTs, suggesting that the blocking effect of the protein becomes the most important contribution; (iv) the highest sensitivities are obtained with nanohybrids prepared using with 2.0 mg mL^{-1} IgG for all MWCNTs concentrations; (v) while the highest sensitivities are mainly obtained with nanohybrids prepared with 3.0 mg mL^{-1} MWCNTs, the reproducibility is the poorest, probably due to some limitation in the exfoliation for such a high amount of MWCNTs; (vi) the MWCNTs concentration that permits the best compromise between sensitivity and reproducibility is 2.5 mg mL^{-1}; and (vii) the IgG concentration that allows to obtain the best compromise between the electrocatalytic activity of the exfoliated MWCNTs and the blocking effect of the protein is 2.0 mg mL^{-1}.

We also evaluated the effect of MWCNT-IgG nanohybrids prepared with 2.5 mg mL^{-1} MWCNTs and different IgG concentrations on the peak potential for AA oxidation at GCE modified with the different nanohybrids (Fig. 5B). The results shown in this figure allows to get the following conclusions: (i) compared to bare GCE ($E_p = 0.545$ V), GCE modified with the nanohybrids prepared with any of the IgG concentrations evaluated shows a large decrease in the oxidation overvoltage, demonstrating once more the preeminence of the electroactivity of MWCNTs over the non-conductive nature of the protein; (ii) for GCE modified with nanohybrids prepared using IgG concentrations between 1.0 mg mL^{-1} and 2.0 mg mL^{-1}, the oxidation peak potential for AA remains almost constant, indicating that, as in the case of hydrogen peroxide, the most important effect is the catalytic activity of the exfoliated MWCNTs; and (iii) for GCE modified with nanohybrids prepared using IgG concentrations higher than 2.0 mg mL^{-1}, there is an increment in the oxidation peak potential since the blocking effect of the protein becomes more important, in agreement with the behavior observed for hydrogen peroxide oxidation. Thus, the optimum conditions to obtain the nanohybrid are 2.5 mg mL^{-1} MWCNTs dispersed in 2.0 mg mL^{-1} IgG.

Effect of the sonication time

Figure S2 shows the sensitivity for hydrogen peroxide oxidation at GCE modified with MWCNT-IgG nanohybrid prepared under the optimal conditions, using different sonication times. The sensitivity increases with the sonication time up to 15 min, indicating that the ultracavitation makes
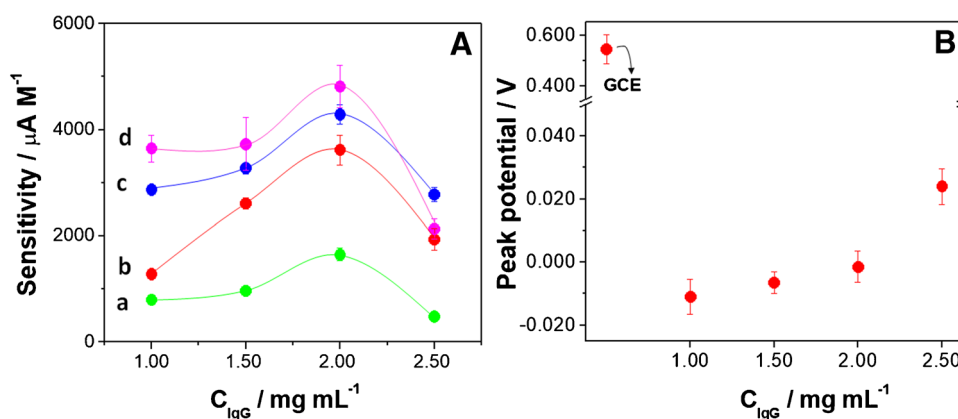

Fig. 5 A) Sensitivities towards hydrogen peroxide obtained from amperometric experiments performed at 0.700 V using GCE modified with MWCNT-IgG nanohybrids prepared with different concentrations of IgG for different MWCNT concentrations: (a) 1.5, (b) 2.0, (c) 2.5, and (d) 3.0 mg mL^{-1}. Supporting electrolyte: 0.050 M phosphate buffer pH 7.40. **B)** Oxidation peak potential for AA obtained from cyclic voltammetric measurements performed at bare GCE and GCE modified with nanohybrids prepared with 2.5 mg mL^{-1} MWCNTs and different IgG concentrations. Other conditions as in Fig. 2

possible the efficient disaggregation of the carbon nanostructures in the presence of the protein. Longer sonication times produce a decrease in the sensitivity, probably due to some conformational changes of IgG that would make the exfoliation less efficient, in agreement with the loosening and unfolding of the protein skeleton reported by Zhang et al. after 30 min of sonication [22].

Therefore, according to the previous results, the selected conditions for the preparation of MWCNT-IgG nanohybrid are 2.5 mg mL^{-1} MWCNTs dispersed in 2.0 mg mL^{-1} IgG and sonicated for 30 min in ultrasonic bath. Under these conditions, the reproducibility obtained from the sensitivity for hydrogen peroxide at 0.700 V, was 4.3% for GCEs modified with the same MWCNT-IgG nanohybrid (for 4 electrodes) and 6.2% for GCEs modified with 5 different nanohybrids.

Biorecognition properties of MWCNT-IgG nanohybrid: immunosensing applications

As it was previously mentioned, the goal of using IgG to prepare MWCNTs-IgG nanohybrids was not only to obtain an efficient exfoliation of the carbon nanotubes, but also, and even more important, to obtain nanohybrids with biorecognition/immunoaffinity properties. Therefore, one critical aspect to evaluate is if the IgG that supports the nanostructures retains its bioaffinity properties after the ultrasonic treatment used to exfoliate the MWCNTs. These properties were checked by studying the interaction of MWCNT-IgG immobilized at GCE with Anti-IgG by EIS using HQ/BQ as redox marker. Figure 6A depicts the charge transfer resistances (R_{ct}) obtained from Nyquist plots for GCE/MWCNT-IgG blocked with BSA (to avoid non-specific interactions), before (black) and after the interaction for 30 min with 0.050 mg mL^{-1} Anti-IgG (red), 0.050 mg mL^{-1} IgG (blue), 0.050 mg mL^{-1} thrombin (green) and 0.050 mg mL^{-1} cytochrome c (magenta). As it can be observed, R_{ct} increases after the interaction of GCE/MWCNT-IgG with Anti-IgG (($3.0 \pm 0.3) \times 10^2$ Ω *versus* $(5.9 \pm 0.2) \times 10^2$ Ω) due to the antigen–antibody interaction between IgG and Anti-IgG, and the consequent blockage of the surface. At variance with this behavior, the interaction of GCE/MWCNT-IgG with 0.050 mg mL^{-1} IgG, thrombin, and cytochrome c produces small changes in the R_{ct} (($3.0 \pm 0.2) \times 10^2$, $(3.3 \pm 0.4) \times 10^2$, and $(2.9 \pm 0.2) \times 10^2$ Ω, respectively), clearly demonstrating that the IgG that supports the MWCNTs really preserves the biorecognition properties despite the treatment used to prepare the nanohybrid. To reinforce this concept, we also evaluated the effect of the interaction time of Anti-IgG with GCE/MWCNT-IgG. Figure 6B shows the bars plot for R_{ct} obtained after increasing the interaction time between GCE/MWCNT-IgG and 0.025 mg mL^{-1} Anti-IgG. The longer the interaction time, the higher the R_{ct}, up to 30 min, due to the immune complex
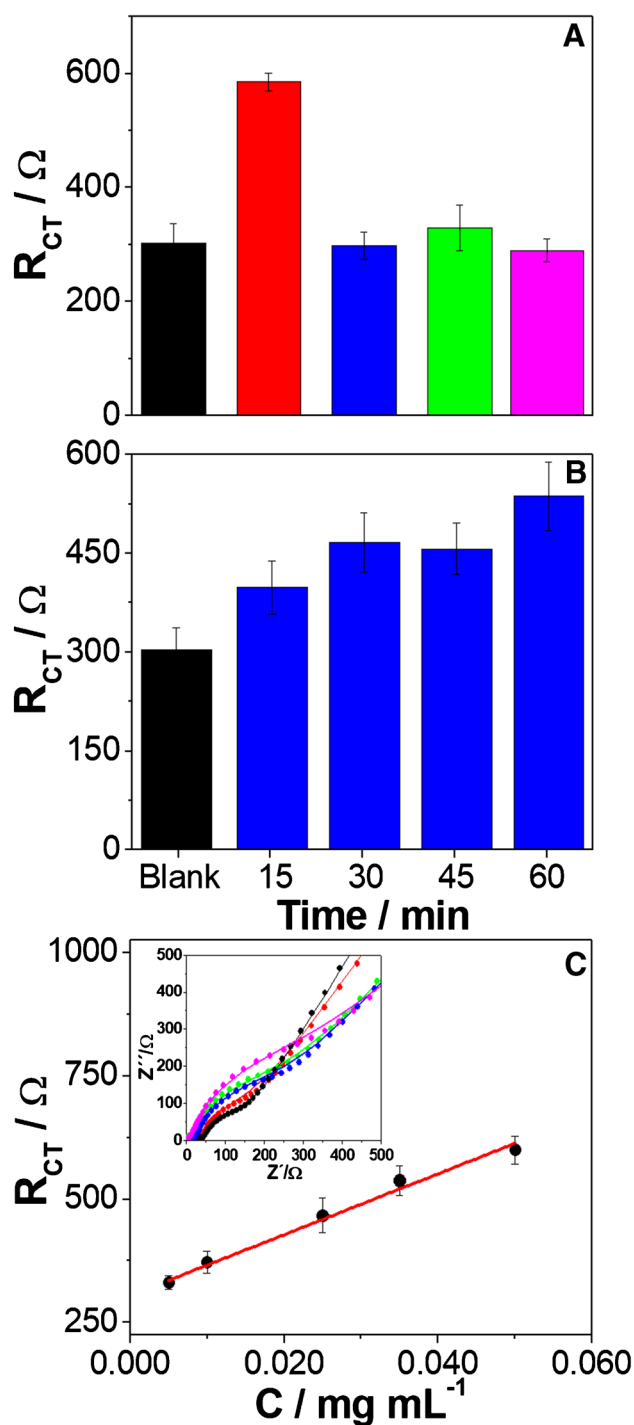

Fig. 6 A) Bars plot for the charge transfer resistances (R_{ct}) obtained from Nyquist spectra for GCE/MWCNT-IgG blocked with BSA before (black) and after the interaction with 0.050 mg mL^{-1} of anti-IgG (red), IgG (blue), thrombin (green), and cytochrome c (magenta). Interaction time: 30 min. Redox marker: 1.0×10^{-3} M HQ/BQ. EIS parameters: potential amplitude, 0.010 V; frequency range, 1.0×10^{-2} to 1.0×10^6 Hz; working potential, 0.200 V. Supporting electrolyte: 0.050 M phosphate buffer solution pH 7.40. **B)** Effect of the interaction time on the R_{ct} obtained at GCE/MWCNT-IgG in the presence of 0.025 mg mL^{-1} Anti-IgG. **C)** Calibration plot obtained from the R_{ct} values of the corresponding Nyquist plots (inset) for increasing concentrations of Anti-IgG (black, 0.005 mg mL^{-1}; red, 0.010 mg mL^{-1}; blue, 0.025 mg mL^{-1}; green, 0.035 mg mL^{-1}; magenta, 0.050 mg mL.$^{-1}$)

formation. For longer times, the R_{ct} remains almost constant, which indicates that the IgG available at the electrode surface for Anti-IgG recognition is saturated. As proof of concept, and with the only goal to demonstrate the potential of the MWCNT-IgG nanohybrid as model bioanalytical platform for further developments of immunosensors, we studied the effect of Anti-IgG concentration on the R_{ct} obtained after a 30min interaction of GCE/MWCNT-IgG with increasing levels of Anti-IgG (Fig. 6C). The proposed model immunosensor displayed a linear relationship between 0.0050 and 0.050 mg mL^{-1}, with a sensitivity of $(5.2 \pm 0.6) \times 10^3$ Ω mL mg^{-1} ($r^2 = 0.990$) and a detection limit of 2 µg mL^{-1} (calculated as $3 \times$ SD/sensitivity, where SD is the standard deviation of the blank signal and S the sensitivity). The reproducibility for 0.005 mg mL^{-1} Anti-IgG was 4.0% using GCEs modified with the same MWCNT-IgG nanohybrid (5 electrodes) and 7.9% using 3 different MWCNT-IgG nanohybrids.

Electroactivity of MWCNT-IgG nanohybrid: sensing applications

As it was previously mentioned, the MWCNT-IgG nanohybrids have two important aspects to consider, the bioaffinity of the resulting platform, through the IgG that supports the MWCNTs, and the electroactivity of the exfoliated MWCNTs. Thus, we also investigated the possible analytical applications of MWCNT-IgG nanohybrid-modified GCEs through the development of a model electrochemical UA sensor. Figure 7A shows the voltammetric response of 1.0×10^{-3} M UA at GCE/MWCNT-IgG. There is a typical irreversible oxidation at 0.300 V with a current of 93 µA. The inset shows the voltammetric behavior of UA at GCE. At variance with GCE/MWCNT-IgG, the oxidation peak potential is 0.600 V, demonstrating the advantages of the electrocatalytic activity of MWCNTs that produces a decrease of 300 mV in the overvoltage for UA oxidation and an enhancement of 7 times in the associated current.

We propose the development of an UA sensor based on the preconcentration at open circuit potential, with LSV-stripping in 0.050 M phosphate buffer solution pH 7.40 after medium exchange. A preconcentration time of 10 min was selected as the best compromise between sensitivity and reproducibility (not shown). Figure 7B displays LSV obtained for different UA concentrations from 5.0×10^{-7} M to 5.0×10^{-6} M. Well-defined oxidation current peaks are obtained for all the studied concentration range (inset), with a linear relationship between current and concentration in the whole range of concentrations, a sensitivity of $(1.37 \pm 0.05) \times 10^6$ µA M^{-1} ($r^2 = 0.996$), and a detection limit of 165 nM (calculated as indicated previously). The reproducibility for 5.0×10^{-6} M UA was 5.0% using the same MWCNT-IgG nanohybrid (3 electrodes) and 9.2% using 3
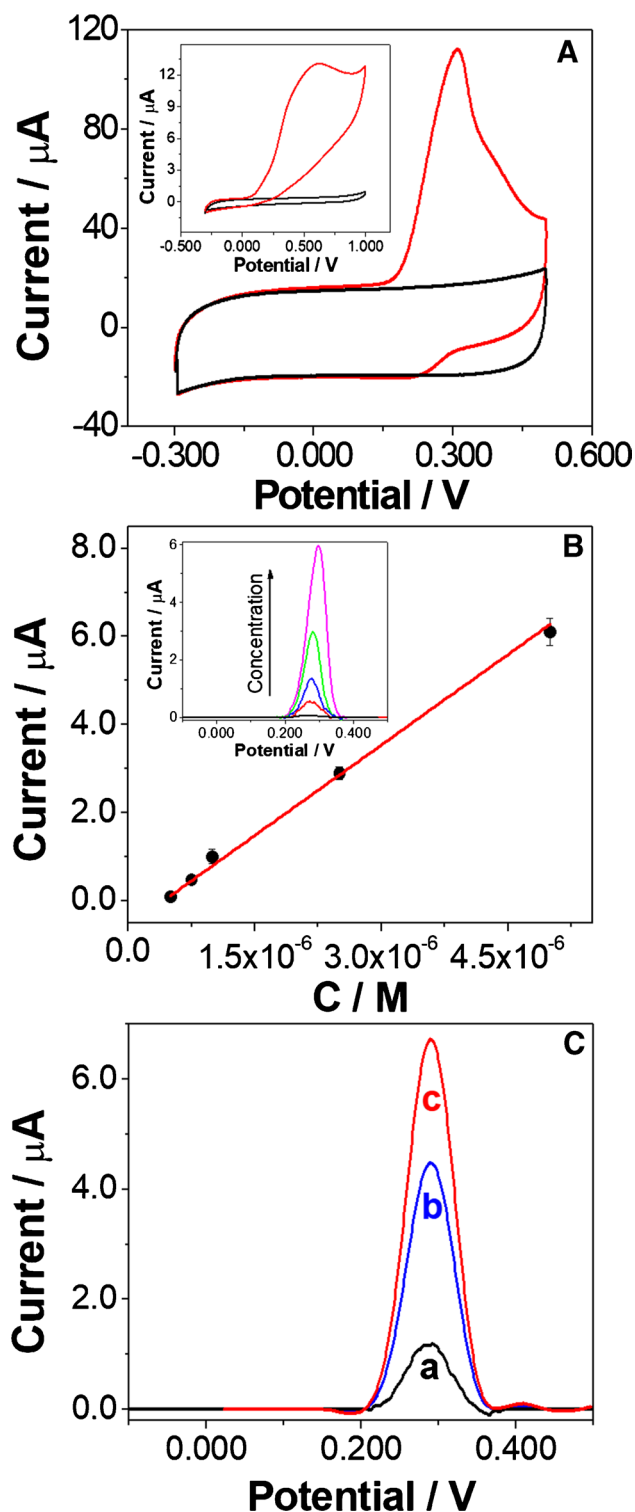

Fig. 7 Cyclic voltammogram for 1.0×10^{-3} M UA solution obtained at GCE/MWCNT-IgG (**A**) and at bare GCE (inset Fig. 7A). Other conditions as in Fig. 2. **B)** Calibration plot for UA obtained from the oxidation peak current of the corresponding LSV-stripping recordings (inset) at GCE/MWCNT-IgG. Preconcentration time: 10.0 min at open circuit potential with medium exchange. Other conditions as in Fig. 2. **C)** LSV-stripping signal for human urine (a) and human urine samples enriched with 2.5×10^{-6} M **b** and $3.5 \times 10.^{-6}$ M **c** of UA at GCE/MWCNT-IgG. All urine samples were diluted 1:1000

different nanohybrids. To evaluate the practical application of the proposed sensor, we challenged it with urine samples. Figure 7C shows LSV recorded for human urine diluted 1:1000 (a) and diluted urine samples enriched with two different UA concentrations, 2.5×10^{-6} M (b) and 3.5×10^{-6} M (c). The recovery percentages obtained with 3 electrodes were 96% and 115% with R.S.D. of 2.6% and 10.4%, respectively, demonstrating the very good analytical performance of the proposed model electrochemical sensor.

Conclusions

This work reports for the first time the use of IgG as exfoliating agent of MWCNTs. The resulting MWCNT-IgG nanohybrid represents a very attractive platform for the development of different (bio)sensing strategies, either based on the biorecognition (immunoaffinity) properties of the IgG that supports the MWCNTs or on the electrocatalytic activity of the exfoliated MWCNTs. Undoubtedly, this new strategy to prepare an immunosensor changes the usual paradigms to build label-free electrochemical immunosensors, with the advantages of an intimate contact of the biorecognition element with the electroactive layer, without any covalent attachment or other immobilization schemes to keep oriented the IgG, paving the way for the development of new immunosensing platforms.

Declarations

Conflict of interest The authors declare no competing interests.

References

1. Suresh I, Selvaraj S, Nesakumar N, Rayappan J, Rayappan JBB, Kulandaiswamy AJ (2021) Nanomaterials based non-enzymatic electrochemical and optical sensors for the detection of carbendazim: a review. Trends Environ Anal Chem 31:e00137. https://doi.org/10.1016/j.teac.2021.e00137

2. Crapnell RD, Banks CE (2021) Electroanalytical overview: utilising micro- and nano-dimensional sized materials in electrochemical-based biosensing platforms. Microchim Acta 188:268. https://doi.org/10.1007/s00604-021-04913-y

3. Sheikhzadeh E, Beni V, Zourob M (2020) Nanomaterial application in bio/sensors for the detection of infectious diseases. Talanta 230:122026. https://doi.org/10.1016/j.talanta.2020.122026

4. Goldoni R, Farronato M, Connelly ST, Tartaglia GM, Yeo WH (2021) Recent advances in graphene-based nanobiosensors for salivary biomarker detection. Biosens Bioelectron 171:112723. https://doi.org/10.1016/j.bios.2020.112723

5. Rivas GA, Rodríguez MC, Rubianes MD, Gutierrez FA, Eguílaz M, Dalmasso PR, Primo EN, Tettamanti C, Ramírez ML, Montemerlo A, Gallay P, Parrado C (2017) Carbon nanotubes-based electrochemical (bio)sensors for biomarkers. Appl Mater Today 9:566–588. https://doi.org/10.1016/j.apmt.2017.10.005

6. Yáñez-Sedeño P, Campuzano S, Pingarrón JM (2017) Carbon nanostructures for tagging in electrochemical biosensing: a review. C – J Carbon Res 3(1):3. https://doi.org/10.3390/c3010003

7. Baig N, Sajid M, Saleh TA (2019) Recent trends in nanomaterial-modified electrodes for electroanalytical applications. Trends Anal Chem 111:47–61. https://doi.org/10.1016/j.trac.2018.11.044

8. Kurbanoglu S, Ozkan SA (2018) Electrochemical carbon based nanosensors: a promising tool in pharmaceutical and biomedical analysis. J Pharm Biomed Anal 147:439–457. https://doi.org/10.1016/j.jpba.2017.06.062

9. Ata MS, Poon R, Syed AM, Milne J, Zhitomirsky I (2018) New developments in non-covalent surface modification, dispersion and electrophoretic deposition of carbon nanotubes. Carbon 130:584–598. https://doi.org/10.1016/j.carbon.2018.01.066

10. Primo N, Gutierrez FA, Luque GL, Dalmasso PR, Gasnier A, Jalit Y, Moreno M, Bracamonte MV, Rubio ME, Pedano ML, Rodríguez MC, Ferreyra NF, Rubianes MD, Bollo S, Rivas GA (2013) Comparative study of the electrochemical behavior and analytical applications of (bio)sensing platforms based on the use of multi-walled carbon nanotubes dispersed in different polymers. Anal Chim Acta 805:19–35. https://doi.org/10.1016/j.aca.2013.10.039

11. Kharlamova MV, Paukov M, Burdanova MG (2022) Nanotube functionalization: investigation, methods and demonstrated applications. Materials 15(15):5386. https://doi.org/10.3390/ma15155386

12. Zhou Y, Fang Y, Ramasamy RP (2019) Non-covalent functionalization of carbon nanotubes for electrochemical biosensor development. Sensors 19:392. https://doi.org/10.3390/s19020392

13. Gutierrez F, Rubianes MD, Rivas GA (2012) Dispersion of multi-wall carbon nanotubes in glucose oxidase: characterization and analytical applications for glucose biosensing. Sens Actuators B Chem 161:191–197. https://doi.org/10.1016/j.snb.2011.10.010

14. Primo EN, Cañete-Rosales P, Bollo S, Rubianes MD, Rivas GA (2013) Dispersion of bamboo type multi-wall carbon nanotubes in calf-thymus double stranded DNA. Colloids Surf B 108:329–336. https://doi.org/10.1016/j.colsurfb.2013.02.028

15. Primo EN, Oviedo B, Sánchez C, Rubianes MD, Rivas GA (2014) Bioelectrochemical sensing of promethazine with bamboo-type multiwalled carbon nanotubes dispersed in calf-thymus double stranded DNA. Bioelectrochem 99:8–16. https://doi.org/10.1016/j.bioelechem.2014.05.002

16. Primo EN, Gutierrez FA, Rubianes MD, Rivas GA (2015) Bamboo-like multiwalled carbon nanotubes dispersed in double stranded calf-thymus DNA as a new analytical platform for building layer-by-layer based biosensors. Electrochim Acta 182:391–397. https://doi.org/10.1016/j.electacta.2015.09.028

17. Gutierrez F, Rubianes MD, Rivas GA (2019) New bioanalytical platform based on the use of avidin for the successful exfoliation of multi-walled carbon nanotubes and the robust anchoring of biomolecules. Application for hydrogen peroxide biosensing. Anal Chim Acta 1065:12–20. https://doi.org/10.1016/j.aca.2019.03.022

18. Gallay PA, Rubianes MD, Gutierrez FA, Rivas GA (2019) Avidin and glucose oxidase-non-covalently functionalized multi-walled carbon nanotubes: a new analytical tool for building a bienzymatic

glucose biosensor. Electroanalysis 31:1888–1894. https://doi.org/10.1002/elan.201900202

19. Gallay P, Eguílaz M, Rivas G (2020) Designing electrochemical interfaces based on nanohybrids of avidin functionalized-carbon nanotubes and ruthenium nanoparticles as peroxidase-like nanozyme with supramolecular recognition properties for site-specific anchoring of biotinylated residues. Biosens Bioelectron 148:111764. https://doi.org/10.1016/j.bios.2019.111764

20. Mujica ML, Rubianes MD, Rivas G (2022) A multipurpose biocapture nanoplatform based on multiwalled-carbon nanotubes non-covalently functionalized with avidin: analytical applications for the non-amplified and label-free impedimetric quantification of BRCA1. Sens Actuators B Chem 357:131304. https://doi.org/10.1016/j.snb.2021.131304

21. Ortiz E, Gallay P, Galicia L, Eguílaz M, Rivas G (2019) Nano-architectures based on multi-walled carbon nanotubes non-covalently functionalized with concanavalin A: a new building-block with supramolecular recognition properties for the development of electrochemical biosensors. Sens Actuators B Chem 292:254–262. https://doi.org/10.1016/j.snb.2019.04.114

22. Zhang T, Tang M, Yao Y, Ma Y, Pu Y (2019) MWCNT interactions with protein: surface-induced changes in protein adsorption and the impact of protein corona on cellular uptake and cytotoxicity. Int J Nanomedicine 14:993–1009. https://doi.org/10.2147/IJN.S191689

23. Lu N, Sui Y, Tian R, Peng YY (2018) Adsorption of plasma proteins on single-walled carbon nanotubes reduced cytotoxicity and modulated neutrophil activation. Chem Res Toxicol 31:1061–1068. https://doi.org/10.1021/acs.chemrestox.8b00141

24. Bard AJ, Mirkin MV (2001) Scanning electrochemical microscopy. Marcel Dekker, New York

25. Wang Y, Bi C (2013) Simultaneous electrochemical determination of ascorbic acid, dopamine and uric acid using poly (tyrosine)/functionalized multi-walled carbon nanotubes composite film modified electrode. J Mol Liq 177:26–31. https://doi.org/10.1016/j.molliq.2012.10.009

26. Eguílaz M, Gutiérrez A, Gutierrez F, González-Domínguez JM, Ansón-Casaos A, Hernández-Ferrer J, Ferreyra NF, Martínez MT, Rivas G (2016) Covalent functionalization of single-walled carbon nanotubes with polytyrosine: characterization and analytical applications for the sensitive quantification of polyphenols. Anal Chim Acta 909:51–59. https://doi.org/10.1016/j.aca.2015.12.031

27. Yang S, Zhang Q, Yang H, Shi H, Dong A, Wang Li YuS (2022) Progress in infrared spectroscopy as an efficient tool for predicting protein secondary structure. Int J Biol Macromol 206:175–187. https://doi.org/10.1016/j.ijbiomac.2022.02.104